

Strongly correlated electrons on frustrated lattices

Peter Fulde,^{1,2} Frank Pollmann,¹ and Erich Runge³

¹Max-Planck-Institut für Physik komplexer Systeme, 01187 Dresden, Germany

²Asia Pacific Center for Theoretical Physics, Pohang, Korea

³Technische Universität Ilmenau, 98683 Ilmenau, Germany

(Dated: November 2, 2018)

We give an overview of recent work on charge degrees of freedom of strongly correlated electrons on geometrically frustrated lattices. Special attention is paid to the checkerboard lattice, i.e., the two-dimensional version of a pyrochlore lattice and to the kagome lattice. For the checkerboard lattice it is shown that at half filling when spin degrees of freedom are neglected and quarter filling when they are included excitations with fractional charges $\pm e/2$ may exist. The same holds true for the three-dimensional pyrochlore lattice. In the former case the fractional charges are confined. The origin of the weak constant confining force is discussed and some similarities to quarks and to string theory are pointed out. For the checkerboard lattice a formulation in terms of a compact U(1) gauge theory is described. Furthermore a new kinetic mechanism for ferromagnetism at special fillings of a kagome lattice is discussed.

PACS numbers:

I. INTRODUCTION

Charge is quantized in nature. Even subparticles like quarks which can't exist separately (quark confinement) carry a quantized charge. It came as a surprise when Su, Schrieffer and Heeger [1,2] pointed out that in trans-polyacetylene $(\text{CH})_n$ excitations may exist that carry only a rational fraction of the electronic charge e , provided those polymer chains are properly doped. Since then we have got used to the fact that in solids fractionally charged excitations may exist which are either deconfined or confined [3,4,5]. It has also become clear that two different types of systems with fractionally charged excitations may occur. One type to which trans-polyacetylene or graphene [4] belong does not require electron interactions for the existence of fractional charges. However lattice degrees of freedom must be included in order that they may form. For the second type of systems electron interactions are crucial for the occurrence of fractional charges. The Fractional Quantum Hall Effect (FQHE) [3] and strongly correlated electrons on geometrically frustrated lattices [5] are examples of that category.

Trans-polyacetylene, graphene and the FQHE are low dimensional systems. Therefore the question arises whether fractionally charged excitations may also appear in three dimensions. Indeed, in 2002 it was suggested by one of us [5] that excitations with charge $\pm e/2$ may exist in pyrochlore and other geometrically frustrated lattices and therefore also in three dimensions. This is of interest since in two dimensional systems like the FQH liquid or graphene excitations with fractional charges obey fractional statistics [6]. They are neither fermions nor bosons but instead anyons. If fractionally charged excitations would always imply fractional or anyonic statistics then one would exclude such excitations in three dimensional systems the reason being that in 3D only fermions or bosons can exist as free particles. The possible existence of fractionally charged excitations in a pyrochlore lattice excludes a simple one to one correspondence between fractional charges and fractional statistics.

We argue that a general prerequisite for fractional charges based on electron interactions are strong short-range correlations and special lattice fillings. Following the general usage, we will simply call a lattice a "frustrated" one when the short-range electronic correlations are incompatible with the lattice structure. It would be more appropriate to speak of "interactions, frustrated by the lattice" but that is not customary.

Here we want to give an overview of recent studies which have been made on charge degrees of freedom of strongly correlated spinless (or fully spin polarized) fermions on frustrated lattices [5,7,8,9,10,11,12,13]. They refer mainly to the pyrochlore lattice and its two dimensional projection, i.e., the checkerboard lattice. But also the kagome lattice will be considered in special cases [14]. The work on the pyrochlore lattice has been stimulated by experimental findings on LiV_2O_4 a transition metal spinel [15]. It was found that it exhibits heavy quasiparticle behavior, a hallmark of strongly correlated electron systems. Note that spinels are of the composition AB_2O_4 with the B sites forming a pyrochlore lattice.

II. CHARGES ON FRUSTRATED LATTICES

In the following we want to concentrate on the crisscrossed checkerboard lattice because a number of features we want to point out are more easily visualized on that lattice than on the pyrochlore lattice. The checkerboard lattice can be considered as a 2D projection of the 3D pyrochlore lattice (see FIG. 1(a)), and we treat lattice points connected by a line as nearest neighbors. Since we are interested in charge degrees of freedom, we disregard the spin. The following Hamiltonian for fully spin polarized electrons or alternatively spinless fermions is assumed to hold

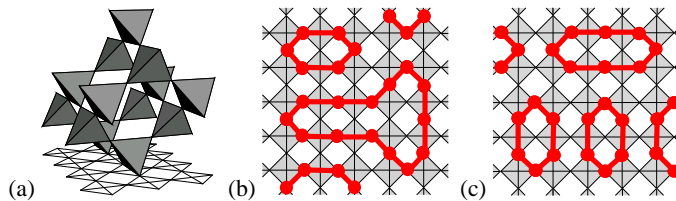


FIG. 1: (a) Checkerboard lattice as 2D projection of the 3D pyrochlore lattice [16]. (b), (c) Two examples of allowed configurations on a checkerboard lattice at half filling. Occupied sites are connected by thick solid lines as guides to the eye.

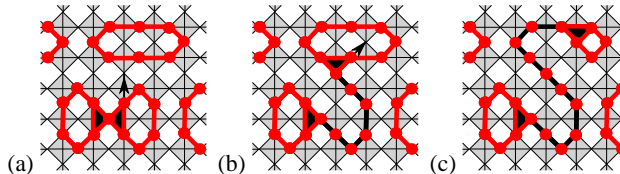


FIG. 2: (a) Adding one particle to the half-filled checkerboard lattice leads to two defects (marked by black triangles) on adjacent crisscrossed squares. (b), (c) Two defects with charge $e/2$ can separate by particle hopping without increase in repulsive energy. They are connected by a string consisting of an odd number of occupied sites.

$$H = -t \sum_{\langle ij \rangle} (c_i^\dagger c_j + H.c.) + V \sum_{\langle ij \rangle} n_i n_j . \quad (1)$$

The operators c_i^\dagger create fermions on sites i . The density operators are $n_i = c_i^\dagger c_i$. We assume a system of N sites filled with $N/2 = \sum_i n_i$ fermions (half filling) and focus on the strong correlation regime, i.e, $|t| \ll V$. Without loss of generality we assume $t > 0$.

A. Ground-state degeneracy:

Consider first the case of $t = 0$. The nearest-neighbor repulsions V are minimized if on each crisscrossed square two of the sites are occupied while two sites remain empty. This we shall call the tetrahedron rule since it applies equally well to the tetrahedra of the pyrochlore structure [17]. All other configurations have a larger potential energy. This implies immediately that the ground state is macroscopically degenerate. More precisely the degeneracy is $N_{\text{deg}} = (4/3)^{\frac{3}{4}N}$ and therefore the same as in the two-dimensional ice model [18]. Two of those configurations are shown in FIGs. 1(b,c) where neighboring occupied sites have been connected by a solid line. Note that a related Klein type spin model on the checkerboard lattice has been studied in Ref. [19] and shown to have a similar ground-state degeneracy. It is noticed that each configuration obeying the tetrahedron rule, which we call *allowed* configurations in the following causes a complete loop covering of the plane. When dynamics is added to the system the time evolution of the loops will give raise to world sheets in a space-time continuum instead of world lines as single particle propagation does. One may speak therefore of a simple form of string theory which is realized here. For an extended discussion of that issue see Section VI.

B. Excitations with charge $\pm e/2$:

Assume that an electron is added to the otherwise half-filled lattice. In that case two neighboring tetrahedra violate the tetrahedron rule because they contain three particles each (see FIG. 2(a)). The energy required for adding the particle is $4V$. Next assume that one particle is hopping to a nearest neighbor site as indicated in FIGs. 2(a,b). The new configuration has the same total repulsive energy as the old one. This can continue as shown in FIG. 2(c) and so on. One notices that the two tetrahedra with three particles have separated without increase in repulsive energy. The charge e of the added particle has thus split into two fractions $e/2$. A similar feature is observed if we add an energy V to the ground-state energy. This suffices to break a loop as indicated in FIG. 3(a,b). We notice a tetrahedron with three particles and one with one particle only.

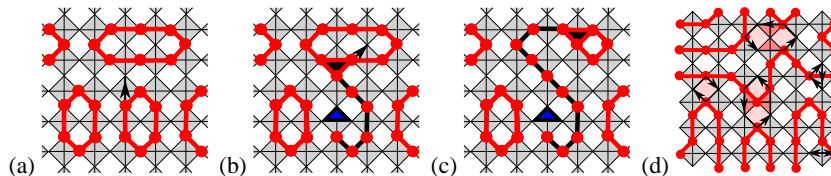


FIG. 3: (a)–(c) Hopping of a particle to a neighboring site: (a) A fractionally charged particle and fractionally charged hole are generated. (b)–(c) The two defects (marked by triangles) with charge $\pm e/2$ can separate without creating additional defects and are connected by a string consisting of an even number of particles. (d) Example of an allowed configuration on a checkerboard lattice at half filling with possible low-order hopping processes [7].

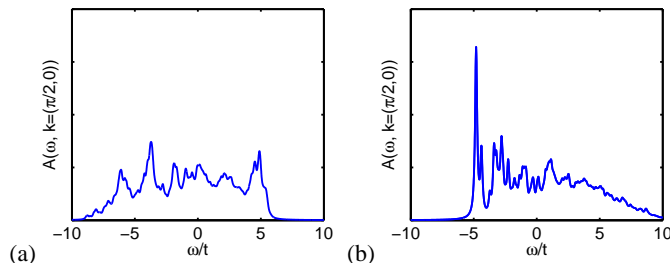


FIG. 4: (a) Spectral function $A(\mathbf{k} = \pi/2, \omega)$ for $V = 25t$ calculated for a $\sqrt{32} \times \sqrt{32}$ cluster for the effective t - g Hamiltonian (9) with (a) $g = 0.01$ and (b) $g = 1$. A Lorentzian broadening $\eta = 0.1t$ is used [8].

Since a tetrahedron with three particles corresponds to a charge $e/2$, the one with one particle only must correspond to a charge $-e/2$. It is an important feature that the fractional charges are always connected by a string of occupied sites, i.e., black lines in FIGs. 2 and 3. In the case of two charges $e/2, e/2$ the string contains always an odd number of sites while for a pair $e/2, -e/2$ the number of sites on the connecting string is always even. When dynamics is added to the system the fractional charges will separate because each of them will gain kinetic energy. The energy of an added particle with momentum \mathbf{k} is therefore

$$E(\mathbf{k}) = 4V + \varepsilon(\mathbf{k}_1) + \varepsilon(\mathbf{k}_2) \quad (2)$$

with $\mathbf{k} = \mathbf{k}_1 + \mathbf{k}_2$. The form of $\varepsilon(\mathbf{k})$ is yet unknown. Similarly the energy of a broken string or vacuum fluctuation is

$$\Delta E = V + \varepsilon(\mathbf{k}) + \bar{\varepsilon}(-\mathbf{k}) \quad (3)$$

where $\bar{\varepsilon}(\mathbf{k})$ is the kinetic energy of the fractional charge $-e/2$.

Fractionally charged excitations are clearly outside the Landau concept of Fermi liquids. Therefore the spectral function does not show a quasiparticle peak like a Fermi liquid does (see FIG. 4(a)). Instead it shows structures which are partially due to finite size effects but have not yet been analyzed in detail. The width of the spectral function is larger than for a particle which is prevented from breaking up into two fractional charges $e/2$. A quasi-particle peak reappears if the ring exchange (see Section III) is so large that confinement (see Section V) becomes strong (see FIG. 4(b)). A more detailed discussion of the spectral function is given in Sect. V. The remaining question is whether the fractional charges are confined or deconfined.

C. Side remark: inclusion of spin

The above considerations referred to spinless fermions. When the spin is included the question arises what happens to it when the charge fractionalizes and falls apart into two pieces. To answer it we have to first generalize the Hamiltonian (1) to the form

$$H = -t \sum_{\langle i,j \rangle \sigma} \left(c_{i\sigma}^\dagger c_{j\sigma} + \text{H.c.} \right) + V \sum_{\langle i,j \rangle} n_i n_j + U \sum_i n_{i\uparrow} n_{i\downarrow}. \quad (4)$$

This is an extended Hubbard Hamiltonian with on-site repulsion U and $n_i = \sum_{\sigma} c_{i\sigma}^\dagger c_{i\sigma}$. It is well known that in the strong correlation limit it can be reduced to a $t - J$ Hamiltonian [20] of the form

$$H_{t-J} = -t \sum_{\langle i,j \rangle \sigma} \left(\hat{c}_{i\sigma}^\dagger \hat{c}_{j\sigma} + \text{H.c.} \right) + V \sum_{\langle i,j \rangle} n_i n_j + \frac{J}{2} \sum_{\langle i,j \rangle} \left(\mathbf{S}_i \mathbf{S}_j - \frac{n_i n_j}{4} \right) \quad (5)$$

where the operators

$$\begin{aligned} \hat{c}_{i\sigma}^\dagger &= c_{i\sigma}^\dagger (1 - n_{i-\sigma}) \\ \hat{c}_{i\sigma} &= c_{i\sigma} (1 - n_{i-\sigma}) \end{aligned} \quad (6)$$

assure that sites are either empty or singly occupied, but never doubly occupied while $J = 4t^2/U$ implies an antiferromagnetic nearest-neighbor interaction. Consequently the strings which connect the fractional charges represent Heisenberg chains with odd (in case of $e/2, e/2$) or even (in case of $e/2, -e/2$) number of sites. But a chain with an odd number of sites has a twofold degenerate ground state and therefore acts like an effective spin $S = 1/2$. In distinction a chain with an even number of sites has a singlet ground state corresponding to $S = 0$. The spin of an added particle is therefore distributed all over the chain and hence delocalized over parts of the sample. This a rather unique physical situation. It should be stressed that all of the above features are not restricted to the checkerboard lattice but hold for the pyrochlore lattice as well where they are less transparent though. A detailed study of the interplay between charge and spin degrees of freedom on the checkerboard lattice at fractional filling factors $1/4$ and $1/8$ can be found in Refs. [21,22,23].

III. DYNAMICAL PROCESSES

The macroscopic degeneracy of the ground state of a half-filled checkerboard- or pyrochlore lattice is lifted when dynamics is introduced, i.e., when t with $|t| \ll V$ is taken into account [7]. This lifting takes place to order t^3/V^2 , because contribution of order t^2/V are equal for all configurations. Note that ring hopping processes of order t^2/V cancel for fermions. But in order t^3/V^2 ring hopping processes connect different configurations with each other. Thus to that order the effective Hamiltonian is of the form

$$H_{\text{eff}} = \frac{12t^3}{V^2} \sum_{\{\odot\}} c_{j_6}^\dagger c_{j_4}^\dagger c_{j_2}^\dagger c_{j_5} c_{j_3} c_{j_1} \quad (7)$$

and the sum is over all hexagons of the lattice. We rewrite this expression in a more pictorial version as

$$\begin{aligned} H_{\text{eff}} &= -g \sum_{\{\odot, \emptyset\}} \left(\left| \begin{array}{c} \odot \quad \odot \\ \hline \odot \quad \odot \end{array} \right\rangle \left\langle \begin{array}{c} \odot \quad \odot \\ \hline \odot \quad \odot \end{array} \right| - \left| \begin{array}{c} \odot \quad \odot \\ \hline \odot \quad \odot \end{array} \right\rangle \left\langle \begin{array}{c} \odot \quad \odot \\ \hline \odot \quad \odot \end{array} \right| + \text{H.c.} \right) \\ &=: -g \sum_{\{\odot, \emptyset\}} \left(\left| B \right\rangle \left\langle \bar{B} \right| + \left| \bar{B} \right\rangle \left\langle B \right| - \left| A \right\rangle \left\langle \bar{A} \right| - \left| \bar{A} \right\rangle \left\langle A \right| \right) \end{aligned} \quad (8)$$

with coupling constant $g = 12t^3/V^2 > 0$. Again the sum is taken over all, i.e., vertically and horizontally oriented hexagons. The symbolic form of H_{eff} is self-explanatory - occupied sites are indicated by a dot, for examples see FIG. 3(d). The minus signs in Eq. (8) result from Fermi commutation rules associated with the ring-hopping processes. They depend on the choice of how the multi-fermion states on the lattice are enumerated. The simple form of Eq. (8) is valid, e.g., for the enumeration used in ?? (along the diagonals) In the case of doping H_{eff} is extended to

$$H_{t-g} = H_{\text{eff}} - t \sum_{\langle ij \rangle} P \left(c_i^\dagger c_j + \text{H.c.} \right) P \quad (9)$$

where the projector P projects onto the subspace of configurations with the smallest possible violations of the tetrahedron rule compatible with the number of doped particles. For one added particle the number of violations is two. We call the extended Hamiltonian the $t - g$ model and consider t and g as independent parameters. Thus we shall assume that the two parameters are not necessarily restricted to $g \ll t$ as required by the strong correlation limit. This is of advantage when numerical calculations are performed. The Hamiltonian (8) and (9) does not include 8-site or 10-site hopping processes which become increasingly important for increasing ratios t/V .

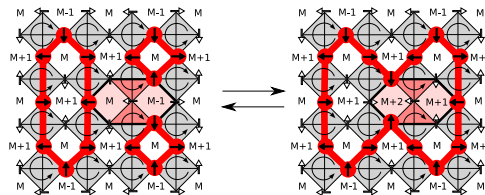


FIG. 5: Height representation for allowed configurations of a $\sqrt{32} \times \sqrt{32}$ checkerboard lattice with periodic boundary conditions at half filling. The height field h (numbers in the non-crossed squares) is uniquely defined for a given configuration up to an additive constant M . The field $\mathbf{f} = \nabla h$ is indicated by small arrows on the lattice sites. Details of the mapping can be found in the text. The effect on the height fields of a ring-exchange process around a hexagon is shown explicitly [7].

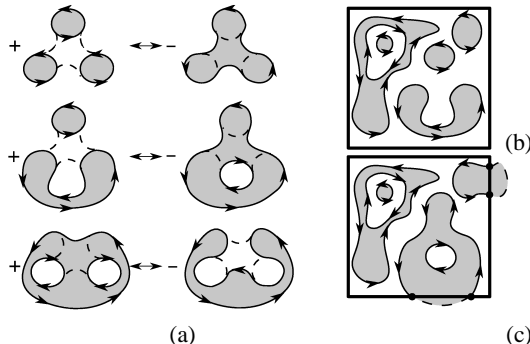


FIG. 6: (a) Changes in loop topologies by ring hopping processes of Type A (see Eq. (8)). (b), (c) Representations of two configurations by fully-packed directed loops [11].

IV. SYMMETRIES AND CONSERVATION LAWS

As pointed out before, H_{eff} lifts the macroscopic degeneracy of allowed configurations, i.e., those which obey the tetrahedron rule. However, the degeneracy is not totally lifted and a residual degeneracy remains. That implies that the total manifold of allowed configurations is divided into different subensembles within which all configurations are connected, but which remain disconnected by H_{eff} . For their identification it is useful to determine the quantities which remain conserved by H_{eff} . It is easy to check that the particle numbers N_1, \dots, N_4 on the four sublattices into which the checkerboard (or pyrochlore) lattice can be divided remain invariant under the operation of H_{eff} . Furthermore, any allowed configuration of the checkerboard lattice can be uniquely represented by a vector field \mathbf{f} with a vanishing discretized lattice version of curl \mathbf{f} . This vector field is obtained for the bipartite lattice by assigning an alternating direction of orientation (i.e., clockwise and counter clockwise) to the tetrahedra, i.e., crisscrossed squares. Each occupied site is associated with an unit vector in the direction of orientation and each empty site with one in opposite direction. This results in a mutual cancellation of the \mathbf{f} vectors on a tetrahedron with two occupied and two empty sites or more generally when a closed loop is formed. From curl $\mathbf{f} = 0$ it follows that the vector field can be represented by $\mathbf{f} = \text{grad } h$ where the scalar field h defines a height field up to an arbitrary constant. The height at the upper (right) and lower (left) boundary of a finite lattice of $N_x \cdot N_y$ crisscrossed squares can differ only by an integer $-N_{y(x)} \leq \kappa_{y(x)} \leq N_{y(x)}$ when periodic boundary conditions are applied. It is the same for all columns (rows) and defines two topological quantum numbers (κ_x, κ_y) . They are invariant under hexagon hopping processes. As seen from FIG. 5 the application of H_{eff} merely changes the local height of two neighboring plain squares by ± 2 . The doublet $(\kappa_x/N_x, \kappa_y/N_y)$ specifies the global slope of the height field.

States with $(\kappa_x, \kappa_y) \neq (0, 0)$ have a broken lattice symmetry and are charge ordered. For example, when $\kappa_x/N_x > 0$ the charge is modulated along a diagonal stripe. Note that violation of the equality $N_1 = N_2 = N_3 = N_4$ also implies a modulation of the charge density.

The different signs in H_{eff} poses a problem when quantum Monte Carlo simulations are applied to the system. Therefore it is of considerable help that in important cases this relative sign can be removed by a proper gauge transformation. The system can then be transformed to a bosonic one. Without going into details which are found in Ref. [11] we describe merely the way this is achieved. We consider allowed configurations with fixed boundary conditions with an even number of fermions on the four boundaries. Open loops are closed as indicated in FIG. 6(c). A given loop covering \mathcal{L} of the plane is processed as follows. We color the background white and alternate the color inside a loop, either from white to dark or reverse. We attach a direction to each loop so that the white colored regime is always to the right of the loop (see FIG. 6(b,c)). Next we count the total number r of clockwise and l of counter-clockwise loops. The three types of topological changes caused by hexagon flipping processes

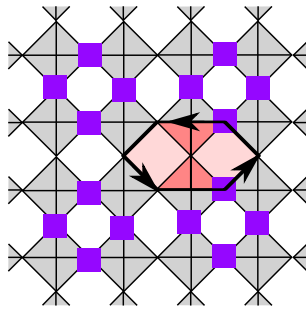


FIG. 7: Ring hopping changes the number of particles by two on sites marked by blue squares by two.

with empty center site are shown in FIG. 6(a). Note that processes with an occupied center site merely deform loops but do not change their topology. The sign change of the processes with an empty center of the hexagon can be cured by transforming the configuration $|\mathcal{L}\rangle$ to

$$|\mathcal{L}\rangle \rightarrow i^{l(\mathcal{L})} (-i)^{r(\mathcal{L})} |\mathcal{L}\rangle . \quad (10)$$

The above considerations need not to apply to periodic boundary conditions where only subensembles with even winding numbers allow for the coloring prescription given above. Even then it may happen that the coloring is reversed by application of H_{eff} while the same loop configuration is recovered. However, from numerical analysis it is found that for tori which preserve the bipartiteness of the lattice the transformation applies indeed to the states of lowest energy. In FIG. 8(a) we compare the energies of a system consisting of 72 sites in which the Fermi sign is taken into account and when it is gauged away, i.e., when the system is treated as a bosonic one. The ground-state energy, the first excited states in the $(\kappa_x, \kappa_y) = (0, 0)$ sector and the weights of the different configurations are the same in both cases. When $(\kappa_x, \kappa_y) \neq (0, 0)$ we find that in some subensembles the ground-state energies are higher for fermions than they are for bosons, i.e., when the fermionic sign is removed by a gauge transformation. All the considerations are limited though to hexagon ring hopping processes and do not apply to higher-order processes.

It should be also mentioned that the sign of g is irrelevant. By multiplying all configurations by a factor i^{σ_p} where σ_p is the number of fermions on the sublattice in FIG. 7, the sign of all matrix elements of H_{eff} is changed. Invariance under this gauge transformation demonstrates a global $g \leftrightarrow -g$ symmetry of the spectrum.

V. CONFINEMENT VS. DECONFINEMENT

The question of confinement of fractional charges is closely related to the form of the ground state of the half-filled lattice. For example, when the ground state is charge ordered then one expects the fractional charges of a doped system to be confined, because a separation of them results in disorder of the ground state. Therefore we discuss first the character of the ground-state wavefunction. The Hamiltonian is given by Eq. (8) but we want to supplement it following Rokhsar and Kivelson [24] by an extra term which counts the number of flippable hexagons. Depending on its sign, configurations with such hexagons are either favoured or partially suppressed. The Hamiltonian which we consider reads therefore

$$H_{g\mu} = H_{\text{eff}} + \mu \sum_{\{\circ, \emptyset\}} (| \langle \text{flippable hexagon} \rangle | + | \langle \text{flippable hexagon} \rangle |) \quad (11)$$

where the sum is over all flippable hexagons with occupied or empty center. Two limiting cases are particularly simple:

- (i) $\mu \rightarrow +\infty$: all configurations without flippable hexagons (frozen configurations) are ground states with energy $E = 0$.
- (ii) $\mu \rightarrow -\infty$: configurations with maximal number of flippable hexagons N_{fl} become ground states. Numerical Monte Carlo calculations for checkerboard lattices up to 1000 sites yield configurations with a "squiggle" type structure [10] or slight variations of it as ground states. The results suggest that in the thermodynamic limit they are all in the $(\kappa_x, \kappa_y) = (0, 0)$ subspace. Due to the large unit cell of the squiggle configuration and the conservation laws the number of different ground states is ten.

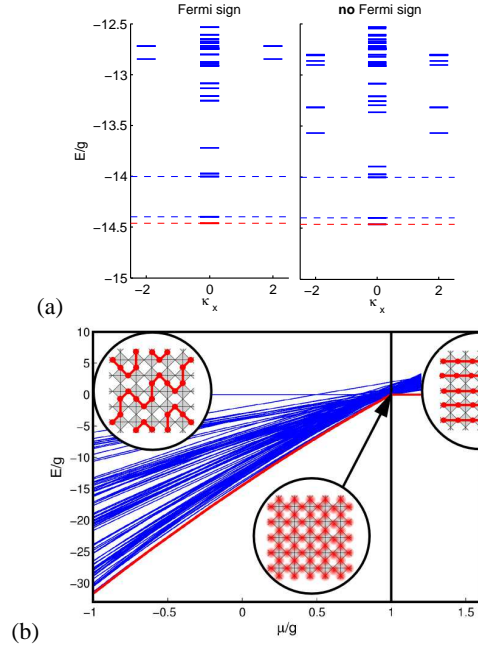


FIG. 8: (a) Ground-state energy and energies of the lowest excited states of the effective Hamiltonian H_{eff} in subspaces with different global slopes $(\kappa_x, \kappa_y) = (\kappa_x, 0)$ for a 72-site cluster. Right side: Same system, but assuming same signs for all matrix elements (“bosonic calculation”). (b) Energies of the ground state and lowest excited states for all subensembles of a 72-site half-filled checkerboard cluster for different values of μ of the g - μ Hamiltonian. Level crossing of ground states occurs only at $\mu = g$. The insets indicate different phases: Maximal flippable plus fluctuations for $\mu < g$, a critical point $\mu = g$ where the ground state is an equally weighted superposition of all configurations, and frozen configurations as ground states for $\mu > g$, [11].

- (iii) $\mu = g > 0$: This is a particularly interesting case because it is exactly solvable [24]. The ground states have energy $E = 0$ and some of them are liquid like. By using the gauge transformation (10) we change the sign of the second term in (8) and rewrite $H_{g=\mu}$ in the form

$$H_{g=\mu} = g \sum_{\{\diamond, \circ\}} [(|\langle \diamond \diamond \rangle\rangle - |\langle \circ \circ \rangle\rangle) \times (\langle \langle \diamond \diamond | - \langle \langle \circ \circ |)] \quad (12)$$

which is a sum over projectors. Therefore all eigenvalues must be non-negative. For each subensemble l the ground-state wavefunction is then given by an equally weighted superposition of all connected configurations $|c_i^{(l)}\rangle$, i.e.,

$$|\psi_0^{(l)}\rangle = A \sum_i |c_i^{(l)}\rangle \quad (13)$$

where A is a normalization prefactor. Using the Perron and Frobenius Theorem (see below), it follows that these are the unique ground states in each subensemble. The coherent superpositions are resonating Valence Bond (RVB) states of the form originally discussed in [25,26]. We want to draw attention that a RVB state is obtained only when a gauge transformation of the form (10) exists which ensures that all off-diagonal matrix elements have the same sign. Otherwise the energy is most likely larger than zero.

Next we explore the phase diagram as function of μ/g by exact diagonalization of $H_{g\mu}$ for clusters up to 72 sites. The details are found in Ref. [10] so that we state here merely the results:

- (i) For $\mu > g$ we find the same features as for $\mu \rightarrow \infty$, i.e., all frozen configurations are ground states.

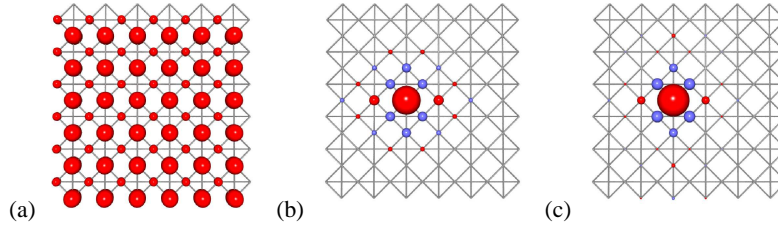


FIG. 9: Half filling: (a) Charge density distribution for one of the two ground states. (b) Corresponding density-density correlation function $C_{i_0 i}^{(l)}$. The site i_0 with average density $2/3$ shows up as the largest dot in the panels (b) and (c). The radius of the dots is proportional to the absolute value. Red or blue color represents a positive and negative value, respectively. (c) Classical density-density correlation function.

- (ii) For $\mu < g$ we find two ground states in subensembles with $(\kappa_x, \kappa_y) = (0, 0)$. They are $(N_1, \dots, N_4) = (6, 6, 12, 12)$ and $(12, 12, 6, 6)$ respectively. They consist of superposition of configurations with maximal number of flippable hexagons and of fluctuations around these configurations. We expect that in the thermodynamic limit the 10-fold degenerate squiggle phase instead of a two-fold degenerate ground state is recovered. The average weight of configurations with maximal number of flippable hexagons decreases as μ increases until at $\mu = g$ all configurations of a subensemble have the same weight.

The energy of the ground state and of the lowest excited states as function of μ/g is shown in FIG. 8 for a cluster of 72 sites.

It is interesting to calculate the density-density correlation function for a 72-site cluster at $\mu = 0$ when one of the two degenerate ground states is used for ψ_0 , i.e.,

$$C_{i_0} = \langle \psi_0 | n_i n_0 | \psi_0 \rangle - \langle \psi_0 | n_i | \psi_0 \rangle \langle \psi_0 | n_0 | \psi_0 \rangle . \quad (14)$$

Here the subscript 0 denotes a site near the center of the cluster. The charge order for the state $N_1, \dots, N_4 = (6, 6, 12, 12)$ yields stripes of average occupation $1/3$ and $2/3$ (see FIG. 9(a)). The result for C_{i_0} is shown in FIG. 9(b). It differs only slightly from the corresponding classical correlation function plotted in FIG. 9(c) which is obtained by setting $t = 0$ and summing over all degenerate configurations.

We are now in the position to discuss the problem of confinement of fractional charges. It is obvious that for $\mu \geq g$, i.e., when the ground state energy is $E = 0$ it does not matter how far two charges $e/2$ of an added particle are separated from each other since the energy is always $4V$. However that is different for $\mu = 0$, the case of physical interest. The energy change can be decomposed into local contributions ε_i which include all hexagon hopping processes involving site i . As seen in FIG. 10(a-c) ε_i increases along the string connection between the two fractional charges (compare with FIG. 2). This is plausible since ring hopping requires alternating empty and occupied sites. In the vicinity of a string of occupied sites these processes are reduced and ε_i increases. The same holds true when a pair $e/2, -e/2$ is separated. Therefore in both cases the fractional charges are confined by a constant confining force, similarly as quarks [27,28]. The energy increase is linear with charge separation. From the numerical results we can deduce an energy increase of $\Delta E \approx 0.2|g|r$ where r is the distance of the fractional charges in units of the site distance a . The energy increase corresponds to a string tension $T = 0.2|g|$. It should be noticed that the restoring force is weak. Assume that $V = 10t$ in which case $g = 0.12$ and $\Delta E = 0.024ta$. The two fractionally charged particles $e/2$ will form a bound state with a radius of order 50 - 100 lattice distances. Thus as soon as there is a small doping concentration the average distance between the fractional charges will be smaller than the diameter of the pairs and a plasma will form. Note that when r exceeds a critical value r_c so that $\Delta E = 0.2g \cdot r_c$ then it is favourable to create fractionally charged particle-hole pairs $e/2, -e/2$ in order to reduce a further energy increase with r . Again, this resembles the generations of quark-antiquark pairs in form of pions, when a quark is separated too far from the other ones.

One would like to know how fractionalization of charge could show up in experiments. One quantity which depends strongly on it is the spectral function $A(\mathbf{k}, \omega) = A^+(\mathbf{k}, \omega) + A^-(\mathbf{k}, \omega)$ which is defined through

$$\begin{aligned} A^+(\mathbf{k}, \omega) &= \lim_{\eta \rightarrow 0^+} -\frac{1}{\pi} \text{Im} \left\langle \psi_0^N \left| c_{\mathbf{k}} \frac{1}{\omega + i\eta + E_0 - H} c_{\mathbf{k}}^\dagger \right| \psi_0^N \right\rangle \\ A^-(\mathbf{k}, \omega) &= \lim_{\eta \rightarrow 0^+} -\frac{1}{\pi} \text{Im} \left\langle \psi_0^N \left| c_{\mathbf{k}}^\dagger \frac{1}{\omega + i\eta - E_0 + H} c_{\mathbf{k}} \right| \psi_0^N \right\rangle . \end{aligned} \quad (15)$$

Here $|\psi_0^N\rangle$ is the ground state with energy E_0 of the half-filled lattice. We have calculated $A(\mathbf{k}, \omega)$ by using the effective H_{t-g} Hamiltonian for a finite cluster and different values of g (see FIG. 4). For small values of g the diameter of the bound pair ($e/2,$

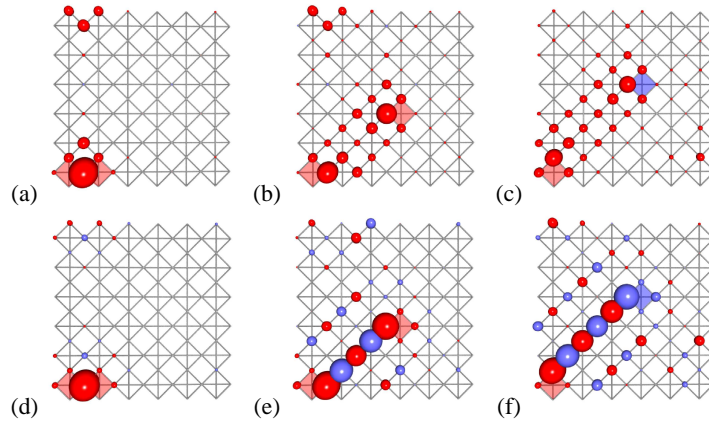


FIG. 10: (a)–(c) Local loss of kinetic energy due to the separation of two (static) fractionally charged defects, i.e., particles or holes (fcp’s marked by light red squares or fch’s marked by dark blue squares). The radii of the circles are proportional to the local energy loss. (d)–(f) Red (blue) circles show an increase (decrease) of the local density (vacuum polarization due to the two fcp’s or the fcp-fch pair).

$e/2$) formed by an added particle exceeds the cluster size. Therefore the fractional charges appear to be deconfined and as seen in FIG. 4(a) there is no quasiparticle peak in $A(\mathbf{k}, \omega)$. This is different when g is sufficiently large, e.g., for $g = 1$. Here the bound pair remains within the finite cluster and therefore a quasiparticle peak does appear (see FIG. 4(b)). The internal degrees of freedom of the bound $(e/2, e/2)$ pair yield additional structure in $A(\mathbf{k}, \omega)$. Note that in FIG. 4(a) as well as 4(b) the bandwidth of $A(\mathbf{k}, \omega)$ is nearly twice as large than as without charge fractionalization in which case it would be $8t$.

Hand in hand with the separation of two fractional charges goes a polarization of the vacuum between the two objects. The modifications of the vacuum in the vicinity of the string connecting the two fractional charges is shown in FIG. 10(d–f). We may consider the vacuum polarization as origin of the confining force.

The above considerations apply to the checkerboard lattice. As far as the pyrochlore lattice is concerned we do not yet know whether fractionally charged particles are confined or deconfined. There are numerical indications that the charges are deconfined here due to the smaller effect of a string of occupied sites on ring hopping. But only detailed numerical work can provide a solid answer [29].

VI. STRINGS AND THEIR TIME EVOLUTION

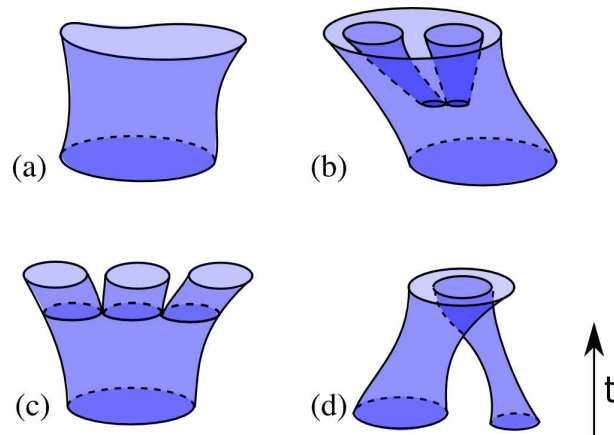


FIG. 11: Continuous representation of loop dynamics due to H_{eff} . (a) Time evolution of loops due to B processes which conserve the topology. (b) - (d) The same for A processes where H_{eff} induces three kinds of topological changes [13].

As it was shown above, when spinless fermions occupy a checkerboard lattice at half filling the strong correlations result in a complete loop covering of the plane. The time evolution of these loops results in world sheets which replace world lines of single particle propagation. Therefore we are dealing here with a simple form of a string theory, a very active and challenging

topic of present days field theory [12,30]. It is interesting to consider the loop dynamics due to H_{eff} in a continuum limit. This is shown in FIG. 11. There are processes denoted by B in Section III which change only the shapes of the loops continuously. They are visualized in FIG. 11(a). In distinction A processes in H_{eff} change the topology of a given loop covering. They were shown in FIG. 6(a) and give raise to a time evolution shown in FIG. 11(b-d).

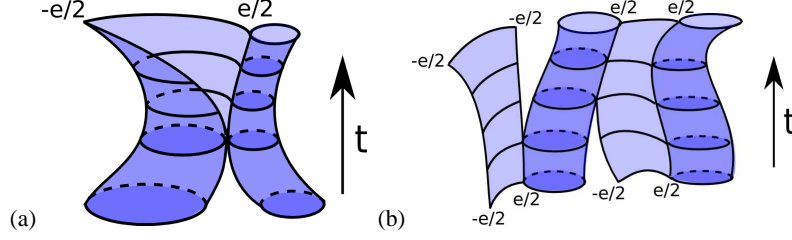


FIG. 12: When an energy $\Delta E > V$ is added to the system a loop is broken and an open string is generated. Thereby one end of the string is touching a closed loop. (a) Time evolution in a continuous representation. (b) Time evolution of two $(e/2, -e/2)$ pairs and formation of e and $-e$ particles.

When an energy $\Delta E > V$ is added to the ground state a loop can break up and a pair of charges $e/2, -e/2$ is generated. This process is shown in FIG. 12(a). When two or more pairs are generated new combinations $e/2, e/2$ and $-e/2, -e/2$ may form. They correspond to the creation of new particles out of the vacuum (ground state). Note that in order that, e.g., the two fractional charges $e/2, e/2$ combine to a particle with charge e they must be situated on different sublattices. This is schematically shown in FIG. 12(b). Fractionally charged particles are always situated at the end of open strings. In case of $e/2$ (but not $-e/2$) the open end is always touching a closed loop. Similar considerations hold for pyrochlore lattices at half fillings.

VII. DERIVATION OF A GAUGE THEORY

The problem of confinement vs. deconfinement of fractional charges on a checkerboard lattice was described in Sect. V. It can also be discussed in terms of a field theory, more specifically a gauge theory. Since the effective Hamiltonian conserves the number of particles on a crisscrossed square the theory is invariant with respect to gauge changes on those squares [12]. This enables us to rewrite the Hamiltonian in form of a $U(1)$ lattice gauge theory and to compare it with that of other models. Similar theories were derived before for the quantum-dimer model [31,32], for a three dimensional spin system [33,34] and for the ice model [35]. The derivation follows the one given by Polyakov [36,37] for compact quantum electrodynamics. By connecting the centers of crisscrossed squares we obtain a square lattice with the particles sitting on links instead of sites. Define for each link $\mathbf{x}, \mathbf{x} + \hat{\mathbf{e}}_j$ between neighboring lattice sites \mathbf{x} and $\mathbf{x} + \hat{\mathbf{e}}_j$ ($j = 1, 2$) a variable $\hat{n}_j(\mathbf{x})$ with integer eigenvalues. In order to express the effective Hamiltonian in terms of $\hat{n}_j(\mathbf{x})$ we first introduce its canonical conjugate, i.e., the phase $\hat{\phi}_j(\mathbf{x}) \in [0, \pi]$. We note that $\exp. [\pm i\hat{\phi}_j(\mathbf{x})]$ acts like a ladder operator. In rewriting ring hopping in terms of $\hat{n}_j(\mathbf{x})$ and $\hat{\phi}_j(\mathbf{x})$ we must ensure that a link is either occupied by one particle or unoccupied. That leads to the following form of the effective Hamiltonian (8)

$$H_{\text{eff}} = \lim_{U \rightarrow \infty} U \sum_{\mathbf{x}_j} \left(\hat{n}_j(\mathbf{x}) - \frac{1}{4} \right) + 2g \sum_{\mathbf{x}_j} \cos \left[\sum_{\{\square \mathbf{B}\}} \pm \hat{\phi} \right] \quad (16)$$

where the first term limits the eigenvalues of $\hat{n}_j(\mathbf{x})$ to 0 and 1 while the second term describes ring hopping. Note that here hexagon ring hopping goes over into hopping around two neighboring squares (double plaquettes) and that the signs of the phases alternate around the polygons. We have assumed that by means of (10) the sign change in (8) has been removed.

Next we introduce staggered gauge and electric fields on the bipartite lattice

$$\begin{aligned} \hat{A}_j(\mathbf{x}) &= (-1)^{x_1+x_2} \hat{\phi}_j(\mathbf{x}) \\ \hat{E}_j(\mathbf{x}) &= (-1)^{x_1+x_2} \left(\hat{n}_j(\mathbf{x}) - \frac{1}{2} \right) . \end{aligned} \quad (17)$$

The theory must incorporate the constraint that each lattice site is touched by exactly two occupied links. This follows from the rule that each tetrahedron contains two particles. Here this constraint reads

$$(\Delta_j \hat{E}_j(\mathbf{x}) - \rho(\mathbf{x})) | \text{Phys} \rangle = 0 \quad (18)$$

with the lattice divergence defined by

$$\Delta_j \hat{E}_j(\mathbf{x}) = \hat{E}_1(\mathbf{x}) - \hat{E}_1(\mathbf{x} - \mathbf{e}_1) + E_2(\mathbf{x}) - \hat{E}_2(\mathbf{x} - \mathbf{e}_2) \quad . \quad (19)$$

It is noticed that the constraint has here the form of Gauss' law. In terms of $\hat{E}_j(\mathbf{x})$ and $\hat{A}_j(\mathbf{x})$ the effective Hamiltonian (16) becomes

$$H_{\text{eff}} = \lim_{U \rightarrow \infty} U \sum_{\mathbf{x}_j} \left(\hat{E}_j^2(\mathbf{x}) - \frac{1}{4} \right) - 2g \sum_{\mathbf{x}_j} \cos \left(\sum_{\square} \hat{A}_\ell(\mathbf{x}) + \sum_{\square} \hat{A}_\ell(\mathbf{x} - \hat{\mathbf{e}}_j) \right) \quad . \quad (20)$$

The oriented sum of the vector potential around one plaquette is

$$\sum_{\square} \hat{A}_\ell(\mathbf{x}) = \hat{A}_1(\mathbf{x}) - \hat{A}_1(\mathbf{x} + \mathbf{e}_2) - \hat{A}_2(\mathbf{x}) + \hat{A}_2(\mathbf{x} + \mathbf{e}_1) \quad . \quad (21)$$

The Hamiltonian resembles the one of compact quantum electrodynamics in 2+1 dimensions [36,37] but is not identical with it. It is interesting that in the latter case two charges are confined and that the energy grows linearly with there distance as it is the case in our model. However, despite of the above mentioned resemblance the physical origin of confinement is different in the two cases. As it turns out the U(1) gauge theory formulation of our model system is gratifying but does not bring much additional insight.

VIII. FERROMAGNETISM GENERATED BY KINETIC PROCESSES

The most common origin of ferromagnetism is spin exchange between electrons. The latter may belong either to different atomic sites or to the same site where intra-atomic exchange is the origin of Hund's rules. Pauli's principle forbids electrons with parallel spins to come too close to each other and reduces this way the mutual Coulomb repulsion. This should be compared with superexchange, the standard mechanism for antiferromagnetism. Here it is the kinetic energy which is optimized in the magnetic phase. Hence it is in general a competition between an optimization of the Coulomb repulsion and of the kinetic energy which favours magnetic order. In passing we mention other sources of ferromagnetism such as RKKY interactions in metals or double exchange, to name of few.

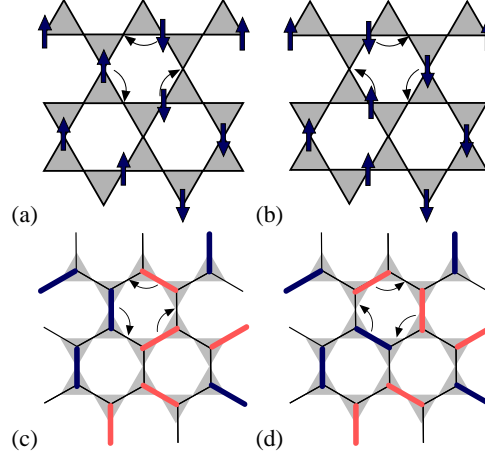


FIG. 13: Panels (a) and (b) show two different allowed configurations on a kagome lattice which fulfill the constraint of zero or one electron per site and one electron of arbitrary spin per triangle. The arrows indicate possible ring-hopping processes. All allowed configurations can be represented by colored dimer coverings on a honeycomb lattice shown in (c) and (d) which is obtained by connecting the centers of triangles. A blue dimer correspond to a spin up and a red dimer to a spin down particle.

It might appear surprising that ferromagnetism may also be caused by purely kinetic processes. We know of two specific examples where this is the case. One is the ferromagnetic ground state discovered by Nagaoka [38]. It is due to a single hole moving in an otherwise half-filled Hubbard system in the limit of infinite on-site repulsion U . The proof is based in a theorem due to Perron and Frobenius. That theorem states (see, e.g., Ref. [39]) the largest eigenvalue of a symmetric $n \cdot n$ matrix with

only positive matrix elements is positive and non-degenerate, while the corresponding eigenvector is nodeless, i.e., we may choose it to have only positive components. The theorem applies only to systems with a finite-dimensional Hilbert space. The same theorem is the basis of three-particle ring exchange in ^3He . In both cases ferromagnetism results from the motion of fermions because the ground state wavefunction is the smoothest in this case (it is nodeless) and has the lowest kinetic energy. Here we want to point out another source of ferromagnetism based on purely kinetic effects. We demonstrate it by considering a partially filled kagome lattice with electrons described by an extended Hubbard Hamiltonian (4). We focus on the case of 1/6 filling implying one electron per triangle. In the limit of $U \rightarrow \infty$ double occupancies of sites are excluded and strong correlations, i.e., $|t| \ll V$ are assumed. When $t = 0$ the ground state is macroscopically degenerate since all configurations with one electron of arbitrary spin orientation per triangle are ground states. For examples see FIG. 13(a,b). By connecting the centers of the triangles of the kagome lattice we obtain as the medial lattice a honeycomb lattice. Here electrons sit on links instead of lattice sites. The different ground-state configurations correspond here to two-colored (spin) dimer configurations (see FIG. 13(c,d)). They are orthogonal because possible wavefunction overlaps are neglected.

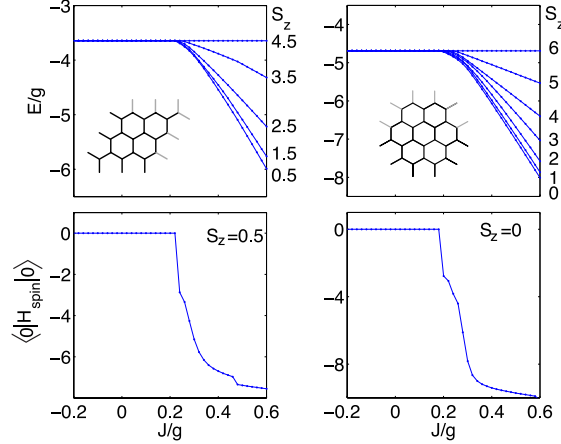


FIG. 14: Exact diagonalization of the two-color dimer model on 24-site honeycomb cluster. The upper panels show the ground-state energies of different S_z sectors as a function of next-nearest neighbor coupling J/g . The lower ones show the expectation values of the spin part of the Hamiltonian. The ground state is denoted by $|0\rangle$ [14].

When we allow for $t \neq 0$ the ground-state degeneracy is lifted. To lowest order of degenerate perturbation theory the effective Hamiltonian acting on the subspace of configurations with precisely one dimer touching each site is written as

$$H_{\text{hex}} = -g \sum_{\{\circ\}\{\blacktriangle\}\bullet} \left(\left(\begin{array}{c} \circ \\ \circ \end{array} \right) \left(\begin{array}{c} \circ \\ \circ \end{array} \right) + \left(\begin{array}{c} \circ \\ \bullet \end{array} \right) \left(\begin{array}{c} \circ \\ \bullet \end{array} \right) + \text{H.c.} \right) \quad (22)$$

where $g = 6t^3/V^2$. The sum is overall hexagon and spin combinations symbolized by the three marks. Note that H_{hex} causes no fermionic sign problem. If we would ignore the spin the model would go over into the quantum dimer model (QDM) studied in Ref. [40]. The ground state of the QDM is known to be three-fold degenerate in the thermodynamic limit. It corresponds to the valence-bond solid (VBS) plaquette phase with broken translational symmetry. Here we are interested in spin correlations and notice that H_{hex} conserves both the total spin S as well as its component S_z . Without proof which is found in Ref. [14] we state that the Perron-Frobenius Theorem is applicable to the present system.

Returning to H_{hex} we remark that by a simple gauge transformation the sign of the plaquette flip in Eq. (22) can be always chosen negative, irrespective of the sign of t [14]. We therefore choose all off-diagonal matrix elements of H_{hex} to be non-positive. But before applying the Perron-Frobenius Theorem we have to discuss the problem of ergodicity. The Hilbert space under consideration is broken into different sectors corresponding to different S_z which are not connected by H_{hex} . Therefore each sector must be considered separately. For the $S_{\text{tot}}^z = S_{\text{max}} = N_e/2$ sector, where N_e is the number of electrons the ground state is unique and fully spin polarized. The situation is more complex for the other sectors with $S_{\text{tot}}^z \neq S_{\text{max}}$. Although it can be shown that a fully spin polarized state is also a ground state in those sectors, it has not been possible to prove convincingly ergodicity, i.e., that the fully spin-polarized ground state is not only one among others. However, the numerical studies on clusters strongly suggest that the ground state is indeed unique.

In order to study the robustness of the kinetic ferromagnetism, we introduce an additional next-nearest neighbor antiferromagnetic interaction so that the total effective Hamiltonian becomes $H_{\text{eff}} = H_{\text{hex}} + H_{\text{spin}}$ with

$$H_{\text{spin}} = J \sum_{\langle\langle ij \rangle\rangle} \left(\mathbf{S}_i \mathbf{S}_j - \frac{1}{4} n_i n_j \right) . \quad (23)$$

Numerical diagonalization of clusters up to 24 sites show that the ground state remains fully spin polarized up to values of $J/g < (J/g)_c \approx 0.2$. This is shown in FIG. 14 which demonstrates a considerable robustness of kinetic ferromagnetism.

A ferromagnetic ground state is also found for a filling factor of $1/3$. The origin of kinetic ferromagnetism in the present examples differs from the ring exchange proposed by Thouless for ${}^3\text{He}$ [41] insofar as there the particles remain at their original location when they cyclically permute while here they actually move around. It differs also from the so-called flat band ferromagnetism of Mielke which he predicted for a kagome lattice with fillings between $5/6$ and $11/12$ [42,43]. In his case any value of $U > 0$ is sufficient and $V = 0$ while in our case $U \rightarrow \infty$ and V/t is large. In Mielke's case a completely flat band in a single particle description of electrons on a kagome lattice influences so strongly the Stoner criterion for the occurrence of ferromagnetism that any value of $U > 0$ leads to a ferromagnetic instability.

-
- ¹ W. P. Su, J. R. Schrieffer, and A. J. Heeger, Phys. Rev. Lett. **42**, 1698 (1979).
 - ² W. P. Su and J. R. Schrieffer, Phys. Rev. Lett. **46**, 738 (1981).
 - ³ R. B. Laughlin, Phys. Rev. Lett. **50**, 1395 (1983).
 - ⁴ C.-Y. Hou, C. Chamon, and C. Mudry, Phys. Rev. Lett. **98**, 186809 (2007).
 - ⁵ P. Fulde, K. Penc, and N. Shannon, Ann. Phys. (Leipzig) **11**, 892 (2002).
 - ⁶ F. Wilczek, *Fractional Statistics and Anyon Superconductivity* (World Scientific, 1990).
 - ⁷ E. Runge and P. Fulde, Phys. Rev. B **70**, 245113 (2004).
 - ⁸ F. Pollmann, P. Fulde, and E. Runge, Phys. Rev. B **73**, 125121 (2006).
 - ⁹ F. Pollmann, J. Betouras, and E. Runge, Phys. Rev. B **73**, 174417 (2006).
 - ¹⁰ F. Pollmann and P. Fulde, Europhys. Lett. **75**, 133 (2006).
 - ¹¹ F. Pollmann, J. Betouras, K. Shtengel, and P. Fulde, Phys. Rev. Lett. **97**, 170407 (2006).
 - ¹² F. Pollmann, J. Betouras, E. Runge, and P. Fulde, J. Magn. Magn. Mat. **310**, 966 (2007).
 - ¹³ P. Fulde and F. Pollmann, Ann. Phys. (Leipzig) **17**, 441 (2008), arXiv:0711.2129.
 - ¹⁴ F. Pollmann, P. Fulde, and K. Shtengel, Phys. Rev. Lett. **100**, 136404 (2008), arXiv:0705.3941.
 - ¹⁵ S. Kondo, D. C. Johnston, C. A. Swenson, F. Borsa, A. V. Mahajan, L. L. Miller, T. Gu, A. I. Goldman, M. B. Maple, D. A. Gajewski, et al., Phys. Rev. Lett. **78**, 3729 (1997).
 - ¹⁶ R. Moessner, O. Tchernyshyov, and S. L. Sondhi, J. Stat. Phys. **116**, 755 (2002).
 - ¹⁷ P. W. Anderson, Phys. Rev. **102**, 1008 (1956).
 - ¹⁸ L. H. Lieb, Phys. Rev. Lett. **18**, 692 (1967).
 - ¹⁹ Z. Nussinov, C. D. Batista, B. Normand, and S. Trugman, Phys. Rev. B **75**, 094411 (2007).
 - ²⁰ A. Auerbach, *Interacting Electrons and Quantum Magnetism* (Springer-Verlag, Berlin, Heidelberg, New York, 1994).
 - ²¹ D. Poilblanc, K. Penc, and N. Shannon, Phys. Rev. B **75**, 220503(R) (2007).
 - ²² D. Poilblanc, Phys. Rev. B **76**, 115104 (2007).
 - ²³ F. Trouselet, D. Poilblanc, and R. Moessner (2007), arXiv:0806.4763.
 - ²⁴ D. S. Rokhsar and A. A. Kivelson, Phys. Rev. Lett. **61**, 2376 (1988).
 - ²⁵ P. W. Anderson, Mater. Res. Bull. **8**, 153 (1973).
 - ²⁶ P. Fazekas and P. W. Anderson, Philos. Mag. **30**, 432 (1974).
 - ²⁷ D. J. Gross and F. Wilczek, Phys. Rev. Lett. **30**, 1343 (1973).
 - ²⁸ H. D. Politzer, Phys. Rev. Lett. **30**, 1346 (1973).
 - ²⁹ O. Sikora, F. Pollmann, N. Shannon, and K. Penc (2008), to be published.
 - ³⁰ B. Zwiebach, *A First Course in String Theory* (Cambridge Univ. Press, Cambridge, 2004).
 - ³¹ E. Fradkin, *Field Theories of Condensed Matter Systems* (Addison-Wesley Publ., Redwood City, 1991).
 - ³² E. Fradkin and S. Kivelson, Mod. Rev. Lett. B **4**, 225 (1990).
 - ³³ M. Hermele, M. P. A. Fisher, and L. Balents, Phys. Rev. B **69**, 064404 (2004).
 - ³⁴ D. L. Bergman, G. A. Fiete, and L. Balents, Phys. Rev. B **73**, 134402 (2006).
 - ³⁵ A. H. C. Neto, P. Pujol, and E. Fradkin, Phys. Rev. B **74**, 024302 (2006).
 - ³⁶ A. M. Polyakov, *Gauge Fields and Strings*, vol. 3 of *Contemporary Concepts in Physics*, 5. print. (Harwood Academic Publishers, 1993).
 - ³⁷ A. M. Polyakov, Nucl. Phys. B **120**, 429 (1977).
 - ³⁸ Y. Nagaoka, Phys. Rev. **147**, 392 (1966).
 - ³⁹ N. Saldanha and C. Tomei, Resenhas **2**, 239 (1995).
 - ⁴⁰ R. Moessner, S. L. Sondhi, and P. Chandra, Phys. Rev. B **64**, 144416 (2001).
 - ⁴¹ D. J. Thouless, Proc. Phys. Soc. **86**, 893 (1965).
 - ⁴² A. Mielke, J. Phys. A: Math. Gen. **24**, L73 (1991).
 - ⁴³ A. Mielke, J. Phys. A: Math. Gen. **25**, 4335 (1992).